phys. stat. sol. (b) **238**, No. 3, 541–547 (2003) / **DOI** 10.1002/pssb.200303186

K-dependent exchange interaction of quadrupole excitons in Cu_2O

G. Dasbach[*,1], **D. Fröhlich**[1], **H. Stolz**[2], **R. Klieber**[1], **D. Suter**[1], and **M. Bayer**[1]

[1] Institut für Physik, Universität Dortmund, 44221 Dortmund, Germany
[2] Fachbereich Physik, Universität Rostock, 18051 Rostock, Germany

Received 24 February 2003, accepted 24 March 2003
Published online 1 August 2003

PACS 71.35.Cc, 78.20.–e., 78.40.Fy

The long- and short-range exchange interaction for the quadrupole allowed transition to the *yellow* 1S orthoexciton in Cu_2O is derived. While the three orthoexciton states still remain degenerate, when treating the exchange up to the order of $\boldsymbol{K}$-linear terms, a fine structure arises when $\boldsymbol{K}$-quadratic terms are included. This splitting is investigated experimentally by high resolution spectroscopy. Exchange contributions of few μeV are resolved and compared to theory. The impact of strain on the exciton fine structure is discussed and evaluated.

1 Introduction The spin properties of excitations in semiconductors are one of the main foci of research in the field of solid state physics. While nowadays most efforts concentrate on spin phenomena in micro- and nanostructures, bulk semiconductors offer a challenging variety of unanswered questions [1].

Spin-spin interaction manifests itself via exchange interaction, which gives rise to a spectral splitting between the spin configurations. While electron–electron exchange is well understood in atomic systems, the picture is of increased complexity for the exciton exchange interaction in semiconductors. The exciton is formed by an excited electron in the conduction band, which is Coulomb coupled to the vacant state (hole) in the valence band. Consequently, the exciton properties are determined by both bands arising from the overlapping atomic orbitals of the lattice constituents. Hence, the lattice symmetry has direct impact on the exciton and its fine structure.

The exchange interaction can be separated into two parts, the long-range contribution closely related to the non-analytical exchange and the short-range part, which is closely related to the analytical exchange [2–4]. Typically exciton exchange interaction in bulk can be treated by an effective exchange Hamiltonian independent of $\boldsymbol{K}$. However, in some cases higher order exchange terms gain importance.

In this paper we will identify contributions of K^2-dependent exchange terms to the *yellow* 1S orthoexcitons in Cu_2O. These states remain degenerate when including K-independent, as well as K-linear exchange. Further, its narrow linewidth permits the resolution even of extremely small exchange shifts.

The degeneracy of the orthoexciton can also be lifted by external perturbations, such as stress. The impact of strain on the observed fine structure is explored in detail and compared to the experimental findings on stress free and stressed samples. A strain Hamiltonian is implemented in the calculations.

2 Experiment

2.1 Experimental setup The optical properties of the *yellow* 1S orthoexciton have been investigated in absorption experiments as sketched in Fig. 1. A ring dye laser *(Coherent 890-21)* is pumped by a

[*] Corresponding author: e-mail: gregor.dasbach@physik.uni-dortmund.de, Phone: +49 231 755 5160, Fax: +49 231 755 3674

frequency doubled Nd:YVO_4-laser. The dye laser is tuned to the exciton resonance ≈ 2.0327 eV. The single frequency laser provides a bandwidth of ≈ 5 neV, while it can be scanned continuously across the resonance in a spectral window of ≈ 0.1 meV. The linear polarization $\boldsymbol{e}(\psi)$ of the laser beam is adjusted by means of a $\lambda/2$-retarder, before it passes trough the polarizer P_1 to ensure precise adjustment of the polarization angle ψ. The laser beam is then focused on the sample, which is placed in a helium bath cryostat ($T = 1.4$ K). The transmitted light passes through a second polarizer P_2, which is oriented parallel to P_1. Finally, the signal is detected by a photodiode, which is connected to an oscilloscope. The photodiode readout is synchronized to the scan ramp of the dye laser. Hence, the sample absorption is monitored as function of excitation energy.

The measurements were performed on high-quality natural Cu_2O-crystals, where two principal types of samples have been investigated: (*i*) Cubic samples with extensions of $\approx$4 mm. (*ii*) Slab shaped samples with a thickness $\leq 100\,\mu$m and lateral sizes of few mm's. In order to insure strain free mounting slab shaped samples were freely standing within their holder (see right section of Fig. 1). The mounting allows to rotate the samples around the vertical axis by an angle φ', which corresponds to an angle φ inside the crystal. The samples were oriented by X-ray diffraction and cut such that $\varphi = 0$ corresponds to a main crystalline axis ($[\bar{1}10], [111], [001]$). For $\varphi \neq 0$ intermediate $\boldsymbol{K}$ directions are investigated.

2.2 Experimental observations So far, the *yellow* 1S orthoexciton was assumed to be threefold degenerate. Taking advantage of the high spectral resolution provided by the single frequency laser, the degeneracy can be put to a test. For this purpose a 4 mm thick cubic crystal was investigated. The orientation of the specimen is such, that for $\varphi = 0$ $\boldsymbol{K}$ points along the $[\bar{1}10]$ direction. The experimental results are shown in Fig. 2. If the polarization points along $[00\bar{1}]$ ($\psi = -36°$) a strong quadrupole absorption is found (Fig. 2 solid trace). No absorption is found in the entire spectral range investigated for $\boldsymbol{e} = [110]$ ($\psi = 54°$, open dots). However, the picture changes drastically if the sample is tilted slightly from $\varphi = 0°$ to $\varphi = 4°$. In this case the strong quadrupole absorption is again found for $\psi = -36°$. More strikingly two sharp lines appear for $\psi = 54°$ (Fig. 2 full dots). Both lines are extremely narrow (FWHM $\approx$1 μeV) with an energy separation of $\approx$4 μeV. Apparently the degeneracy of the orthoexciton has been lifted. The origin of the splitting will be discussed in the following.

3 Impact of perturbations The degeneracy of the orthoexciton states can be lifted by strain. The data of Fig. 2 were obtained from a sample with extensions of 4 mm. Due to the relatively large size of the specimen, an inhomogeneous strain distribution across the sample might be expected. The central parts should be less affected by strain than the outer sections of the cube, where cutting and polishing can give rise to an increased stress. Hence, the splitting should depend on the sample section being probed.

To clarify this issue the absorption spectrum was recorded for illumination of the specimen in the sample center (solid line) and close to the sample edge (dotted line). In Fig. 3 $\boldsymbol{K}$ is slightly tilted from $[\bar{1}10]$ and the polarization is $\psi = 54°$ (close to $\boldsymbol{e} = [110]$). Hence, the situation is identical to that

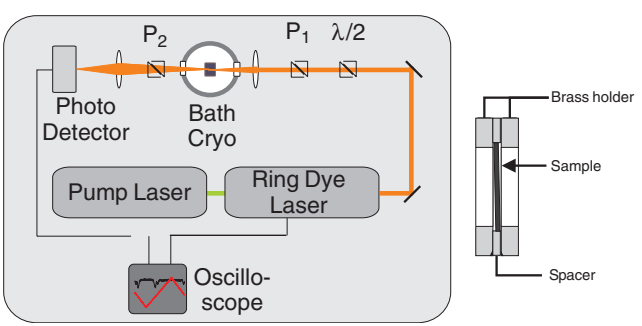

Fig. 1 (online colour at: www.interscience.wiley.com) Left: Experimental setup, as described in the text. Right: Schematic of sample holder. Two brass plates with openings are separated by a spacer slightly thicker than the sample, which guarantees a stress-free mounting.

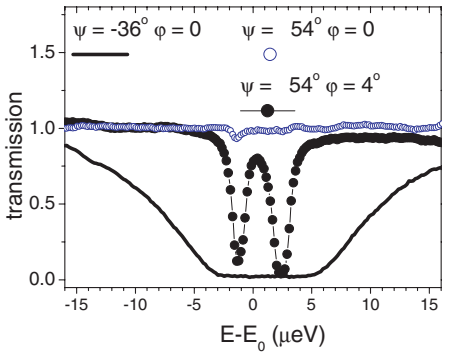

Fig. 2 (online colour at: www.interscience.wiley.com) Spectrally resolved transmission spectra of a 4 mm thick Cu_2O cube. $\boldsymbol{K}$ is along $[\bar{1}10]$ at $\varphi = 0$. The solid trace (open dots) gives the spectrum for $\boldsymbol{e} = [00\bar{1}]$ ($\boldsymbol{e} = [110]$). The full dots give the transmission spectrum for $\varphi = 4°$ (rotation around the [111] axis) and $\psi = 54°$.

given by the dotted trace in Fig. 2 (full dots). In both spectra two lines with a splitting of $\approx$4 μeV are found. The comparison of the spectra shows that the spectral shifts of the exciton energies are insignificant as compared to the total splitting. Nevertheless discrepancies can be found when the illumination spot is moved close to the sample edge.

In such a thick sample a rather large volume of the specimen is probed, even with a focused beam. Thus, strain could give rise to an inhomogeneous broadening of the lines. However, our data show that for the laser going through the sample center the lines remain extremely narrow (FWHM $\leq$ 1 μeV) and Lorentzian. For the beam travelling along the edge of the sample, the line shape of the high energy line deviates from a Lorentzian and the shoulder on the high energy side can arise from a strained section of the sample. The data show that slight stress can be found in the surface regions of the sample. However, this does not have a significant impact on the fine structure and can be disregarded when the laser beam strikes the center of a thick sample. From these considerations we can conclude, that the observed fine structure does not arise from strain.

4 *K*-quadratic exchange As external perturbations can be excluded as origin of the orthoexciton splitting, we focus on other sources. The first candidate is exchange interaction, which can be approached by symmetry considerations: For the *yellow* 1S orthoexciton the hole is in the valence band of Γ_7^+ type, while the electron can be attributed to the Γ_6^+ conduction band. The combination of Γ_7^+ symmetry and Γ_6^+ symmetry leads to two irreducible representations

$$\Gamma_7^+ \otimes \Gamma_6^+ = \Gamma_2^+ \oplus \Gamma_5^+. \tag{1}$$

Γ_2^+ describes the paraexciton, which is a pure spin triplet state. The paraexciton is optically forbidden for dipole as well as quadruple transitions. The three Γ_5^+ states form the orthoexcitons, which are allowed for optical quadrupole transitions. The conventional K-independent exchange splits the orthoexciton from the paraexciton by an energy of 12 meV [6].

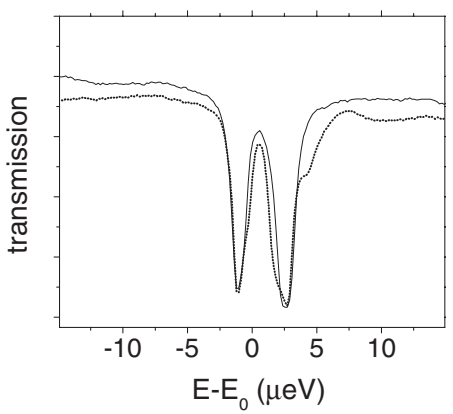

Fig. 3 Spectrally resolved transmission spectra for $\varphi = 4°$ (rotation around the [111] axis, $\boldsymbol{K}(\varphi = 0) = [\bar{1}10]$) and $\psi = 54°$ (close to $\boldsymbol{e} = [110]$). The spectra are recorded for excitation in the sample center (solid line) and excitation close to the edge of the sample (dotted line).

As we are facing a splitting among the three-fold orthoexciton states and K-independent exchange leaves those states degenerate, exchange contributions of higher order in K have to be taken into account. Due to the inversion symmetry of the lattice (point group O_h) K-linear contributions vanish. This puts the focus on terms of order K^2, which will now be derived.

The exchange interaction for excitons with the spatial charge distributions $\rho(\boldsymbol{r_1})$ and $\rho'(\boldsymbol{r_2})$ can be expressed as [3]:

$$J_{\mathrm{ex}} = \delta_{\boldsymbol{K},\boldsymbol{K'}} \sum_{\boldsymbol{R}} \exp(i\boldsymbol{K}\cdot\boldsymbol{R}) \int\int \frac{\rho^*(\boldsymbol{r}_1)\,\rho'(\boldsymbol{r}_2)\,\mathrm{d}\boldsymbol{r}_1\,\mathrm{d}\boldsymbol{r}_2}{|\boldsymbol{r}_1+\boldsymbol{r}_2-\boldsymbol{R}|}. \tag{2}$$

With the Fourier transform

$$M(\boldsymbol{K}) = \int \mathrm{d}\boldsymbol{r}\,\rho(\boldsymbol{r})\exp(-i\boldsymbol{K}\cdot\boldsymbol{r}) \tag{3}$$

J_{ex} can be written as

$$J_{\mathrm{ex}} = \delta_{\boldsymbol{K},\boldsymbol{K'}}\,\frac{4\pi}{\Omega}\sum_{\boldsymbol{n}}\frac{M^*(\boldsymbol{K}+\boldsymbol{K_n})\cdot M'(\boldsymbol{K}+\boldsymbol{K_n})}{(\boldsymbol{K}+\boldsymbol{K_n})^2}\,, \tag{4}$$

with the reciprocal lattice vectors $\boldsymbol{K}_n$ and the wave vector $\boldsymbol{K}$.

4.1 Long-range exchange The long-range part of the exchange interaction ($\boldsymbol{K}_n = 0$) is given by [3]

$$J'_{\mathrm{ex}} = \delta_{\boldsymbol{K},\boldsymbol{K'}}\,\frac{4\pi}{\Omega}\,\frac{M^*(\boldsymbol{K})\,M'(\boldsymbol{K})}{\boldsymbol{K}^2}\,. \tag{5}$$

We expand $\exp(-i\boldsymbol{K}\cdot\boldsymbol{r})$ into the spherical harmonics $Y_{l,m}$ [7]

$$\exp(-i\boldsymbol{K}\cdot\boldsymbol{r}) = \sum_{l=0}^{\infty}\sum_{m=-l}^{m=+l} 4\pi(-i)^l\,j_l(Kr)\,Y^*_{l,m}(\alpha,\beta)\,Y_{l,m}(\theta,\phi)\,. \tag{6}$$

Here θ and ϕ (α and β) are the spherical angles of $\boldsymbol{K}$ ($\boldsymbol{r}$) with respect to the cubic axes. $j_l(Kr)$ are the modified Bessel functions of order l.

Inserting Eq. (6) into Eq. (3) and changing the order of summation and integration, we obtain

$$M(\boldsymbol{K}) = \sum_{l=0}^{\infty}\sum_{m=-l}^{m=+l} 4\pi(-i)^l\int \mathrm{d}\boldsymbol{r}\,\rho(\boldsymbol{r})\,j_l(kr)\,Y^*_{l,m}(\alpha,\beta)\,Y_{l,m}(\theta,\phi) \tag{7}$$

for the charge distribution. As we are dealing with quadrupole states, we can concentrate on $l = 2$. The Bessel function of $l = 2$ is given by $j_2(Kr) = (Kr)^2/15 + \ldots$, where terms of higher order are neglected. We thus get

$$M(\boldsymbol{K}) = \sum_{m=-2}^{m=+2} 4\pi(-i)^2\,\frac{K^2}{15}\,\sqrt{\frac{5}{4\pi}}\,q_m Y_{2,m}(\theta,\phi)\,, \tag{8}$$

with the quadrupole moments [7]

$$q_m = \sqrt{4\pi/5}\int \mathrm{d}\boldsymbol{r}\,r^2 Y^*_{2,m}(\alpha,\beta)\,\rho(\boldsymbol{r})\,. \tag{9}$$

Using Eq. (5) and Eq. (8) the quadrupole-quadrupole long-range exchange interaction can be written as

$$J^Q_{\mathrm{ex}} = \delta_{\boldsymbol{K},\boldsymbol{K'}}\,\frac{16\pi^2}{45\Omega}\,K^2\sum_{m_1=-2}^{2}\sum_{m_2=-2}^{2} q^*_{m_1}q'_{m_2}Y^*_{2,m_1}(\theta,\phi)\,Y_{2,m_2}(\theta,\phi)\,. \tag{10}$$

To obtain J^Q_{ex} in the basis of $|\Gamma^+_{5yz}\rangle, |\Gamma^+_{5zx}\rangle, |\Gamma^+_{5xy}\rangle$ we proceed with a basis transformation. In the new basis the quadrupole moments can be written as $q_2 = iC_0\alpha_{xy}$, $q_1 = -C_0(\alpha_{xz} - i\alpha_{yz})$, $q_0 = 0$ with $C_0 = \sqrt{5/24\pi}\,Q_0$, Q_0 denoting the amplitude of the transition quadrupole and α_{ik} the expansion coefficients of the exciton wavefunction in the $|\Gamma^+_{5yz}\rangle, |\Gamma^+_{5zx}\rangle, |\Gamma^+_{5xy}\rangle$ basis. We finally find for the long-

range quadrupole–quadrupole exchange

$$J_{\mathrm{ex}}^{Q} = \Delta_Q \cdot \frac{1}{K^2} \begin{pmatrix} K_z^2 K_y^2 & K_z^2 K_x K_y & K_z K_x K_y^2 \\ K_z^2 K_x K_y & K_z^2 K_x^2 & K_x^2 K_y K_z \\ K_z K_x K_y^2 & K_x^2 K_y K_z & K_x^2 K_y^2 \end{pmatrix}. \tag{11}$$

In contrast to dipole excitons, the long-range part of the quadrupole–quadrupole exchange scales as K^2 and is analytic at $K = 0$. The first attempt to calculate the quadrupolar exchange interaction was recently done by Moskalenko et al. [8]. In their treatment the quadrupolar interaction between the exciton states was given as an effective dipole–dipole interaction, but did not take the off-diagonal interaction matrix elements into account. As these are of the same magnitude as the diagonal terms, their results differ from our full treatment.

4.2 Short-range exchange We now turn to the derivation of the K^2 short-range exchange contributions. These are obtained by the method of invariants [3]. The Hamiltonian has to be invariant under the operations of the cubic group and retain its scalar form [9]. The wavevector transforms like Γ_4^-, while the spin operators transform as Γ_4^+. The total exchange Hamiltonian can be split into independent invariant representations (J_i). Each exchange representation is formed by the electron and hole spin operators. The exchange of order K^2 decomposes into contributions of Γ_1^+, Γ_3^+, Γ_4^+, and Γ_5^+ symmetry.

- The term of Γ_1^+ symmetry is expressed in the cartesian Γ_5^+ basis as

$$J_1 = \Delta_1 \cdot \begin{pmatrix} K_x^2 + K_y^2 + K_z^2 & 0 & 0 \\ 0 & K_x^2 + K_y^2 + K_z^2 & 0 \\ 0 & 0 & K_x^2 + K_y^2 + K_z^2 \end{pmatrix} = \Delta_1 K^2 \cdot \mathbf{1}. \tag{12}$$

As it is proportional to the identity matrix, it causes a uniform spectral shift and it contributes to spatial dispersion where it can be interpreted as a correction to the effective mass. As Δ_1 cannot be determined independently in the current experiment, it will be included in the energy E_0 of the degenerate orthoexciton state.

- The Γ_3^+ contribution is given by

$$J_3 = \Delta_3 \cdot \begin{pmatrix} 2K_x^2 - K_y^2 - K_z^2 & 0 & 0 \\ 0 & 2K_y^2 - K_x^2 - K_z^2 & 0 \\ 0 & 0 & 2K_z^2 - K_x^2 - K_y^2 \end{pmatrix}. \tag{13}$$

Again all off-diagonal elements vanish and no mixing of the Γ_5^+ states occures. However, the $\boldsymbol{K}$-dependence allows the determination of the J_3 contribution (Δ_3).

- The Γ_4^+ contribution vanishes.
- The Γ_5^+ term is given by

$$J_5 = \Delta_5 \cdot \begin{pmatrix} 0 & K_x K_y & K_x K_z \\ K_x K_y & 0 & K_y K_z \\ K_x K_z & K_y K_z & 0 \end{pmatrix}. \tag{14}$$

As for the long-range term (Eq. (10)), a $\boldsymbol{K}$-dependent mixing of the $|\Gamma_{5yz}\rangle$,$|\Gamma_{5zx}\rangle$ and $|\Gamma_{5xy}\rangle$ states is expected.

Summarizing, there are three terms, which determine the orthoexciton splittings: the long-range quadrupole–quadrupole interaction J_{ex}^{Q}, and the short-range contributions J_3 and J_5. The quadrupole amplitudes $QA_{1,2,3}(\boldsymbol{e}, \boldsymbol{K})$ of the three transitions are given by [11]

$$\begin{pmatrix} QA_1 \\ QA_2 \\ QA_3 \end{pmatrix} = \begin{pmatrix} k_y e_z + k_z e_y \\ k_z e_x + k_x e_z \\ k_x e_y + k_y e_x \end{pmatrix}. \tag{15}$$

5 Comparison of theory to the experimental data After having derived the $\boldsymbol{K}^2$ quadrupole exchange, we can compare it to our data. According to Eq. (14) for $\boldsymbol{K} = [\bar{1}10]$ and $\boldsymbol{e} = [110]$ QA is zero for all transitions, while strong absorption is found for $\boldsymbol{e} = [00\bar{1}]$, this agrees with the experiment (open dots and solid line in Fig. 2). For this K-direction exchange interaction lifts the degeneracy of all three states with the new eigenenergies: $E_1 = E_0 + \frac{1}{2}(\Delta_3 - \Delta_5), E_2 = E_0 + \frac{1}{2}(\Delta_3 + \Delta_5)$, and $E_3 = E_0 - \Delta_3 + \frac{1}{4}\Delta_Q$. However, states E_1 and E_3 should only be observable, when $\boldsymbol{K}$ is slightly tilted from $\boldsymbol{K} = [\bar{1}10]$ and these states become weakly allowed. This exactly matches the observations of Fig. 2.

As the exchange interaction crucially depends on $\boldsymbol{K}$ further investigations along various K-directions have to show whether the splitting indeed arises from exchange interaction. For this purpose samples cut along different crystalline axes have been investigated. For $\boldsymbol{K} = [001]$ we find a twofold high energy level and a single low energy state. For this K-direction the orthoexciton states are shifted to $E_1 = E_2 = E_0 - \Delta_3$, and $E_3 = E_0 + 2\Delta_3$ by exchange interaction. Since in the experiments the high energy state is degenerate, we conclude that Δ_3 must be negative.

The level structure changes for $\boldsymbol{K} = [111]$ where the exchange energies are expected to be $E_1 = E_2 = E_0 - \frac{1}{3}\Delta_5$, and $E_3 = E_0 + \frac{2}{3}\Delta_5 + \frac{1}{3}\Delta_Q$. As predicted, only two lines appear in the experiment. By a polarization analysis the low energy state is found to be degenerate, while a single level is found at high energies in the experiment. From the quantitative evaluation of the exchange parameters we obtain $\Delta_Q = 5\,\mu\text{eV}$, $\Delta_5 = 2\,\mu\text{eV}$ and $\Delta_3 = -1.3\,\mu\text{eV}$. These parameters give a consistent description of the experimental data for all investigated $\boldsymbol{K}$-directions.

6 Modelling strain induced shifts The quantitative analysis is hampered by the strong broadening of the intense exciton resonances (Fig. 2). The broadening is suppressed in samples of thickness $<100\,\mu\text{m}$. Therefore it is desirable to investigate the fine structure in such slab shaped samples.

We have seen above, that the surface areas of the samples are not totaly strain free. For the slab shaped samples these effects gain importance and stress induced perturbations can no longer be disregarded. Using polarization microscopy, stress inside the specimen is made visible. In Fig. 4 sections of two samples are shown. The sample on the left shows clear signatures of strain, which is inhomogeneous across the sample. The picture on the right shows a weakly strained sample (the bright spots arise from dirt particles). Although the sample is rather homogenous, weak traces of strain can still be found.

In the following we will clarify if such residual strain has significant impact on the orthoexciton fine structure. The impact of residual strain can be approached by symmetry considerations: The strain tensor $\vec{\vec{\varepsilon}}$ possess the same symmetry as the K^2-exchange terms. Therefore the effect of strain on Γ_5^+-states is described by the same types of operators as given in equations (12) to (14), where each k_i has to be replaced by ε_i. Hence, the strain can be quantified by three parameters δ_1, δ_3, and δ_5.

In Fig. 5 the spectral positions of the orthoexciton resonances are studied vs. φ with $\boldsymbol{K} = [111]$ ($\varphi = 0$) and rotation around $[11\bar{2}]$. The experimental data are given by the open squares in both panels. In panel (a) the exchange splittings according to the parameter set obtained on unstrained samples are shown (open dots). Apparently the calculations do not match the data. In panel (b) the calculations include strain of Γ_3^+ and Γ_5^+ type, while the exchange parameters remain unaltered and good agreement with the experiment is found.

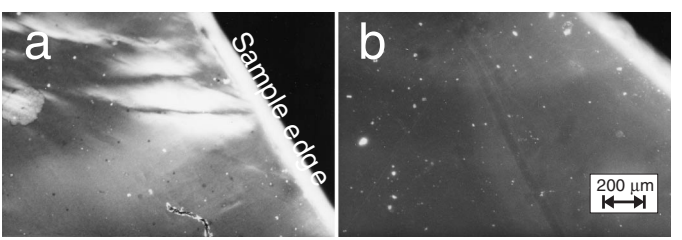

Fig. 4 Microscopic pictures of two slab shaped samples. The specimens were positioned between two crossed polarizers. Hence bright areas indicate, where the sample is stressed. The bright white line is the sample edge. The dark areas in the upper right corners give a reference without sample. Both samples are about 100 µm thick.

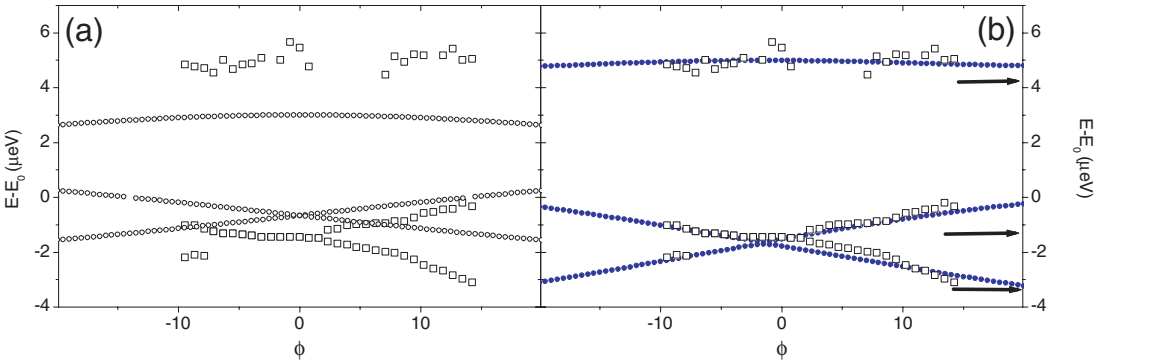

Fig. 5 (online colour at: www.interscience.wiley.com) Dispersion of the orthoexciton resonances vs. φ (rotation around the $[11\bar{2}]$ axis) measured on a 30 μm thick Cu_2O slab. The experimental data are given by open squares. In panel a) calculations based on the parameters $\Delta_Q = 5$ μeV, $\Delta_5 = 2$ μeV and $\Delta_3 = -1.3$ μeV are plotted (open dots). In panel b) the calculations also include strain of Γ_3^+ and Γ_5^+ type, keeping the exchange parameters fixed (full dots). Arrows mark the strain induced line shifts.

Obviously, even residual stress has a significant impact on the fine structure for such thin samples. However, the $\boldsymbol{K}^2$ exchange terms are of crucial importance. The strain induced shift depends on the crystalline axis, but not on $\boldsymbol{K}$. In the present experiment strain causes a spectral shift of the exciton states, which has about the same magnitude as the exchange splitting (see arrows in Fig. 5b). Consequently, it only causes shifts of E_1, E_2, and E_3, but does not contribute to their dependence on φ. The $\boldsymbol{K}$-dependent characteristics arise purely from $\boldsymbol{K}$-square exchange and the parameter set obtained on the cube shaped samples is therefore confirmed.

7 Conclusions In conclusion, we have demonstrated K^2-dependent exchange interaction among the orthoexciton states of the *yellow* 1S excitons in Cu_2O. The data are described by an exchange Hamiltonian and the parameters $\Delta_Q = 5$ μeV, $\Delta_5 = 2$ μeV and $\Delta_3 = -1.3$ μeV. The impact of strain is discussed for thin samples ($d_{\text{sample}} < 100$ μm), as well as thick samples ($d_{\text{sample}} > 4$ mm). While stress is of minor importance for thick cubic samples, the fine structure is affected by strain in slab shaped samples. It leads to a spectral offset of each state, while the $\boldsymbol{K}$-dependence of E_1, E_2, and E_3 purely arises from K^2-dependent exchange.

Acknowledgements We are grateful to H. J. Weber for fruitful discussions concerning the sample preparation. The work was supported by the Deutsche Forschungsgemeinschaft in the Graduiertenkolleg *Materialeigenschaften und Konzepte zur Quanteninformationsverarbeitung.*

References

[1] For an overview see: Semiconductor Spintronics and Quantum Computation, edited by D. D. Awschalom, D. Loss, and N. Samarth (Springer, Berlin, 2002).
[2] R. S. Knox, Solid State Phys. **5**, 25 (1963).
[3] K. Cho, Phys. Rev. B **14**, 4463 (1976).
[4] H. Fu, L.W. Wang, and A. Zunger, Phys. Rev. B **59**, 5568 (1999).
[5] V. T. Agekyan, phys. stat. sol. (a) **43**, 11 (1977).
[6] G. Kuwabara, M. Tanaka, and H. Fukutani, Solid State Commun. **21**, 599 (1977).
[7] J. Schwinger et al., Classical Electrodynamics (Perseus Books, Reading, Mass., 1998).
[8] S. A. Moskalenko, A. I. Bobrysheva, and E. S. Kiselyova, phys. stat. sol. (b) **213**, 377 (1999).
[9] J. M. Luttinger, Phys. Rev. **102**, 1030 (1956).
[10] G. Koster et al., Properties of the thirty-two point groups (M.I.T. Press, Cambridge, Mass., 1963).
[11] R. J. Elliott, Phys. Rev. **124**, 340 (1961).